Structural and optical study of nickel doped ZnO nanoparticles and thin films for dye sensitized solar cell applications

S. THAKUR, J. KUMAR*, J. SHARMA , N. SHARMA, P. KUMAR[a]
Department of Physics, Arni University, Kangra (Himachal Pradesh)
[a]*Center for Nanoscience and Nanotechnology, DAVIET, Jalandhar (Punjab)*

Nanocrystals and thin films of pure and Ni doped Zinc Oxide nanoparticles have been prepared by solution route spin-coating process. Crystalline phases, morphology and optical absorption of Ni doped ZnO nanoparticles/Thin films were studied by X-ray diffraction, Atomic Force Microscopy and UV visible spectrophotometer. X ray studied revealed that Ni doped ZnO crystallised in Hexagonal wurtzite structure. The size strain plot (SSP) method was used to study the individual contributions of crystallite size and lattice strain on the peak broadening of Ni doped ZnO nanoparticles. Physical parameters such as strain, stress and energy density values were calculated more precisely for all reflections corresponding to the wurtzite hexagonal ZnO phase in the range of 20-60^0 (2 values) by using the SSP method. The optical gap was found to increase from 3.47 to 3.51 eV with the increase in Ni doping. The obtained AFM characteristics are in accordance to the results got by means of measurements of X-Ray diffraction spectroscopy.

(Received January 21, 2013; accepted September 18, 2013)

Keywords: A1. Ni-doping, A1. Optical band-gap, A3. Sol–gel method, B1. ZnO thin films

1. Introduction

Semiconductors with dimensions in the nanometer realm are important because their electrical, optical and chemical properties can be tuned by changing the size of particles. Optical properties are of great interest for application in optoelectronics, photovoltaic and biological sensing. Various chemical synthetic methods have been developed to prepare such nanoparticles [1]. Zinc Oxide (ZnO) is a unique material with a direct band gap (3.37 eV) and large exciton binding energy of 60 meV. Because of its exceptional optical and electrical properties, zinc oxide has been extensively used in many technological applications such as near-UV emission, thin film transistors, gas sensors, transparent conductor, Biomedical and piezoelectric application [2-6]. In addition to these applications ZnO also shows its potential in Dye Sensitized solar cells. Dye sensitized solar cells (DSSCs) are a new type of metal oxide wide-band-gap solar cells composed of a semiconductor photoanode absorbed dye molecules, and a counter electrode, and an electrolyte between photoanode and counter electrode. In recent years, a dye sensitized titanium dioxide (TiO_2) solar cell made by Grätzel et al. has been considered as a cost-effective alternative to traditional solar cells. Nowadays, the TiO_2 DSSC modified with other semiconductor materials, such as zinc oxide, is widely investigated to improve the cell performance. ZnO posses a wide band gap, low resistance and high light trapping characteristics that make them useful in solar cells applications.

Most of the ZnO crystals have been synthesized by traditional high temperature solid state method which is energy consuming and difficult to control the particle properties [7]. ZnO nanoparticles can be prepared on a large scale at low cost by simple solution based methods, such as chemical precipitation, sol-gel synthesis, and solvothermal/hydrothermal reaction [8]. Hydrothermal technique is a promising alternative synthetic method because of the low temperature process and very easy to control the particle size [9]. The hydrothermal process have several advantage over other growth processes such as use of simple equipment, catalyst-free growth, low cost, large area uniform production, environmental friendliness and less hazardous [10]. The low reaction temperatures make this method an attractive one for microelectronics and plastic electronics. This method has also been successfully employed to prepare nanoscale ZnO and other luminescent materials [11]. The particle properties such as morphology and size can be controlled via the hydrothermal process by adjusting the reaction temperature, time and concentration of precursors [12]. The present study focuses on the hydrothermal synthesis of ZnO nanopowders/thin films concentration of the precursors and time of growth on its properties.

2. Experimental

2.1 Sample synthesis and geometric characterization

The synthesis of ZnO nanoparticles was carried out by hydrothermal method. The starting materials, $Zn(CH_3COO)_2.2H_2O$ and $Ni(NO_3)_2.6H_2O$ solution were

prepared as follows: Solution A: 1M Zn $(CH_3COO).2H_2O$ dissolved in distilled water and ethanol in 80:20 and Solution B: Different concentrations of $Ni(NO_3)_2.6H_2O$ in a distilled water and ethanol in 80:20. Mixing these solutions has resulted into solution C. The experiment was performed at room temperature. Ammonia solution was added into the solution C drop by drop. The initial solution contains milky colored precipitates of Zinc acetate at low concentration of ammonia. Separately, a buffer solution was prepared by dissolving appropriate amounts of sodium hydroxide. The buffer solution was then added drop wise to the vigorously stirred solution C until the turbidity appears. The turbid solution was then used to prepare thin films using spin coater and to extract precipitates. The resulting precipitates are collected, washed, with distilled water and dried at 500°C for 1 hour in muffle furnace and ground to fine power using agate mortar and pestle.

Thin films of the above-mentioned pure and Ni doped ZnO samples were prepared by spin coating method. Well cleaned glass slides were used as substrates. The solution was dropped onto glass substrate, which was rotated at 300 rpm for 30 s. After deposited by spin coating, the films were dried at several conditions for 5 min to evaporate the solvent and remove organic residuals. The procedure from coating to drying was repeated fifteen times until the desired thickness of sintered films was reached. The films were then annealed at 350^0C for 1 hour.

The crystal structure and the particle size of the thin films were identified using a X-ray diffractometer (XRD Model: D8 Focus). A UV-2501 UV–vis spectrophotometer (SHIMADZU, Japan) with an integrating sphere was used to directly record diffuse reflectance spectra of the pure and Ni doped ZnO.

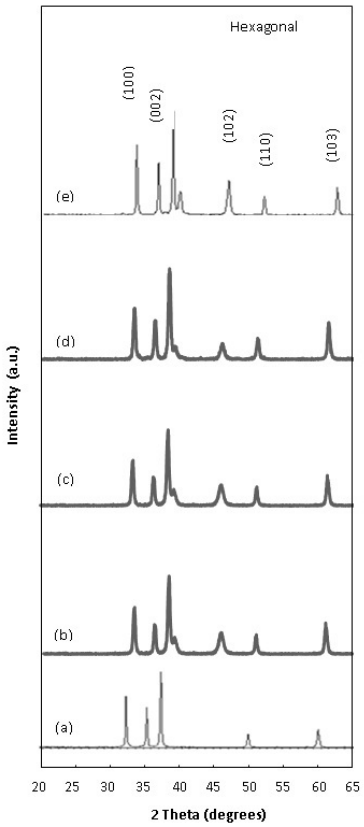

Fig. 1. The XRD pattern of Pure ZnO -NPs and Ni doped ZnO- NPs heated at 500^0 C.(a) Pure ZnO- NPs, (b) $Ni_{0.1}$ -doped ZnO- NPs, (c) $Ni_{0.2}$ - doped ZnO- NPs, (d) $Ni_{0.3}$ -doped ZnO –NPs, (e) $Ni_{0.4}$ -doped ZnO NPs.

3. Results and discussion

3.1 XRD Analysis

Fig. 1 shows the XRD patterns of Ni-doped the prepared sample. It is clearly seen that the FWHM of the reflection peaks decreases with increased dopent cations, indicating growth of the crystallinity or changes in the crystal strains [13]. There is also a negligible shift in peak positions, and their FWHM obviously decreased for the samples that were doped with different concentration of Ni compared to the un-doped ZnO-NPs. By replacing Ni with Zinc in the lattice, the strain changed as shown in the peak shift.

In this study, hydrothermal method was used to prepare pure and Nickel doped ZnO ($Zn_{1-x}Ni_xO$, where x = 0.1 to 0.4). A absolute evaluation of the mean crystalline size of the compounds obtained from powder XRD procedures is reported. The strain due to lattice deformation associated with the different concentration of nickel doped ZnO and pure ZnO heated at 500^0 C was estimated by the size- strain plot method (SSP), which provides information on the stress- strain relation and the strain □ as a function of energy density [14].

Wurtzite lattice parameters such as the values of d, the distance between adjacent planes in the Miller indices (hkl), lattice constants a, b, and c, interplaner angle (the angle ϕ between the planes (h_1 k_1 l_1), of spacing d_1 and the plane (h_2 k_2 l_2) of spacing d_2), and unit cell volumes were calculated from the Lattice Geometry equation presented below [15] .The lattice parameters of the powder samples heated at 500^0 C with different concentration are summarized in Table 1.

$$\frac{1}{d^2} = \frac{4}{3}\left(\frac{h^2+hk+k^2}{a^2}\right)+\frac{l^2}{c^2} \quad (1)$$

$$V = \frac{\sqrt{3}a^2c}{2} = 0.866a^2c \quad (2)$$

$$\cos\theta = \frac{h_1h_2+k_1k_2+\frac{1}{2}(h_1k_2+h_2k_1)+\frac{3a^2}{4c^2}l_1l_2}{\sqrt{(h_1^2+k_1^2+h_1k_1+\frac{3a^3}{4c^2}l_1^2)(h_2^2+k_2^2+h_2k_2+\frac{3a^2}{4c^2}l_2^2}} \quad (3)$$

Table 1. The structure parameter of un-doped and Ni-doped ZnO NPs heated at 500 ^{0} C.

Compound	2theta	hkl	d	Structure	Lattice parameter(nm)	V(nm^3)	Cosϕ
ZnO	31.78 34.43	(100) (002)	2.857 2.604	Hexagonal	a = 3.25 c/a = 1.60	47.66	0
$Ni_{0.1}Zn_{0.99}O$	31.81 34.45	(100) (002)	2.812 2.603	Hexagonal	a = 3.24 c/a = 1.60	47.27	0
$Ni_{0.2}Zn_{0.98}O$	31.75 34.39	(100) (002)	2.815 2.605	Hexagonal	a = 3.25 c/a = 1.60	47.57	0
$Ni_{0.3}Zn_{0.97}O$	31.74 34.43	(100) (002)	2.811 2.602	Hexagonal	a = 3.25 c/a = 1.61	47.41	0
$Ni_{0.4}Zn_{0.96}O$	31.81 34.48	(100) (002)	2.811 2.599	Hexagonal	a = 0.325 c/a = 1.61	47.41	0

Size- Strain plot method

A better evaluation of the size-strain parameter can be obtained by considering an average size-strain plot (ssp), which has the advantage that less weight is given to data from reflections at high angles, where the precision is usually lower. In this approximation, it is assumed that the crystallite size profile is described by a lorentzian function and the strain profile by a Gaussian function [16]. Accordingly, we have

$$(d_{hkl}\beta_{hkl}\cos\theta)^2 = \frac{K}{D}\left(d^2_{hkl}\beta_{hkl}\cos\theta\right) + (\epsilon/2)^2 \qquad (4)$$

Where k is the constant that depends on the shape of the particles: for spherical particles it is given as ¾. In Fig. 2, the term $(d_{hkl}\beta_{hkl}\cos\theta)^2$ is plotted with respect to $(d^2_{hkl}\beta_{hkl}\cos\theta)$ for the all orientation peaks of pure and doped ZnO-NPs. The particle size is determined from the slope of the linearly fitted data and the root of the y-intercept gives the strain. According to Hook's law, a linear proportionality between the stress and strain as given as σ = Y ϵ, where σ is the stress of the crystal and Y is the modulus of elasticity or Young's modulus, for a significantly small strain. This equation deviates from this linear approximation with increasing strain [17].

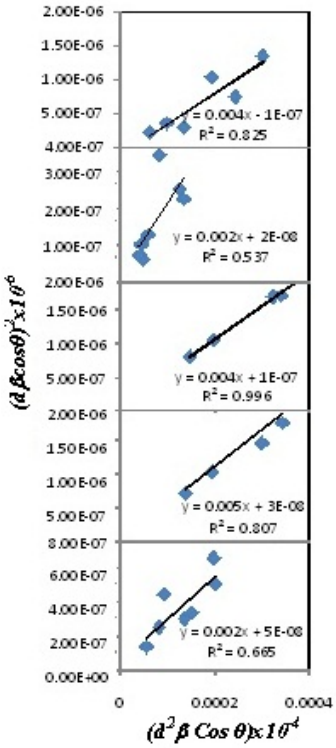

Fig. 2. The SSP plot of Ni – doped and undoped ZnO NPs heated at 500 ^{0} C (a) undoped ZnO NPs (b) $Ni_{0.1}$ doped ZnO NPs (c) $Ni_{0.2}$ doped ZnO NPs (d) $Ni_{0.3}$ doped ZnO NPs (e) $Ni_{0.4}$ doped ZnO NPs. The particle size is achieved from the slop of the linear fitted data and the root of y- intercept gives the strain.

For a hexagonal crystal, Young's modulus is given by the following relation:

$$Y_{hkl} = \frac{\left[h^2 + \frac{(h+2k)^2}{3} + \left(\frac{al}{c}\right)^2\right]^2}{s_{11}\left(h^2 + \frac{(h+2k)^2}{3}\right) + s_{33}\left(\frac{al}{c}\right)^4 + (2s_{13}+s_{44})\left(h^2 + \frac{(h+2k)^2}{3}\right)\left(\frac{al}{c}\right)^2} \qquad (5)$$

Where s_{11} , s_{13} ,s_{33} , s_{44} are the elastic compliance of ZnO with values of 7.858×10^{-12} , -2.206×10^{-12} , 6.940×10^{-12}, 23.57×10^{-12} m^2N^-, respectively [18]. Young's modulus for the pure ZnO and Ni doped ZnO was calculated, and then the stress was calculated according to the equation (4). For an elastic system that follows Hooke's law, the energy density u (energy per unit) can be calculated from $u = (\epsilon^2 Y_{hkl})/2$. The results obtained from the size strain plot model are summarized in Table 2.

Table 2. Geometric parameters of pure and Ni doped ZnO heated at 500°C.

Compound	D(nm)	$\epsilon \times 10^{-4}$	$Y \times 10^9$	$\sigma \times 10^6$	$U \times 10^3$
ZnO	163.0	10	127.25	127.25	63.625
$Ni_{0.1}Zn_{.99}O$	234.37	7.5	127.25	108.067	40.52
$Ni_{0.2}Zn_{0.98}O$	64.10	2.5	127.25	36.0225	4.50
$Ni_{0.3}Zn_{0.97}O$	29	12.5	127.25	180.1125	112.25
$Ni_{0.4}Zn_{0.96}O$	313.33	2.5	127.25	36.0225	39.76

3.2 AFM analysis

A comparison of AFM image of Ni doped ZnO (ZnO:Ni) films grown on glass substrates is shown in Fig. 3. The surface morphologies of the films are presumably same, i.e., Ni- doped ZnO films present pillar-like growth characteristic. 2D-AFM images show grain growth with increased Ni content. The average sizes of nanoparticles are comparable with those obtained from the XRD studies.

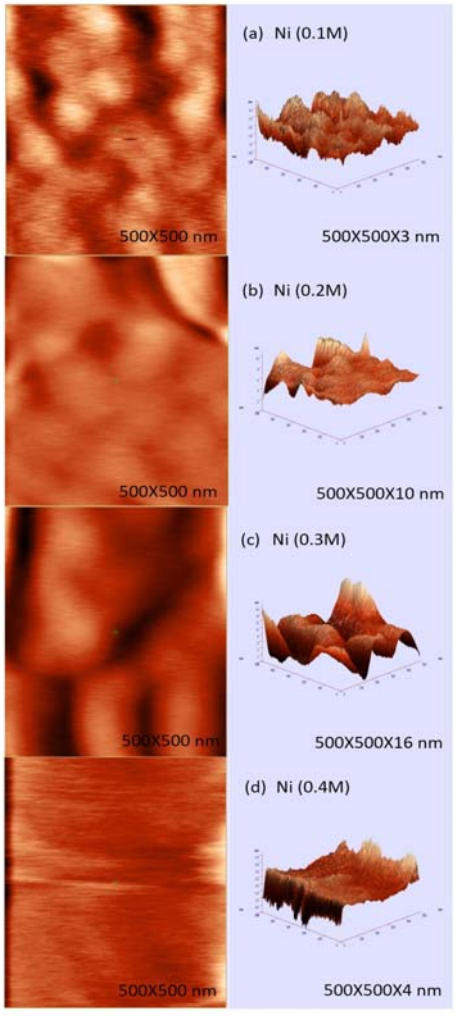

Fig. 3. AFM 2D (500x500nm) and 3D topography images of Ni- doped ZnO (ZnO:Ni) films at different concentration.

3.3 Optical analysis

Diffuse reflectance spectra were recorded to estimate the optical band gap of the pure and nickel doped zinc oxide with different concentrations (Zn_{1-x} Ni_x O, where (x = 0.1 to 0.4)). Difused reflectance spectroscopy (DRS) on powders or pallets is roughly analogous to transmission measurements on thin films. Fig. 4 shows the plot for the percentage of reflection as a function of band gap energy ($h\upsilon$) of the nanoparticles synthesized via hydrothermal method. Doped ZnO samples exhibited absorption peaks in the visible region in addition to the absorption edge, since the samples containing nickel ions will have bands from crystal-field transitions of ions in tetrahedral coordination. As an example, the absorption spectrum of Ni^{2+} doped ZnO shows the mid-band-gap states appearing at about 419 nm, corresponding to the d-d transition bands, which are characteristic of Ni (II) with tetrahedral symmetry. In the case of Ni doped ZnO, absorption peaks are expected to arise due to electronic transitions from the $^3T_1(F)$ ground state to the $^3T_1(P)$ state for the tetrahedral Ni(II).[19]

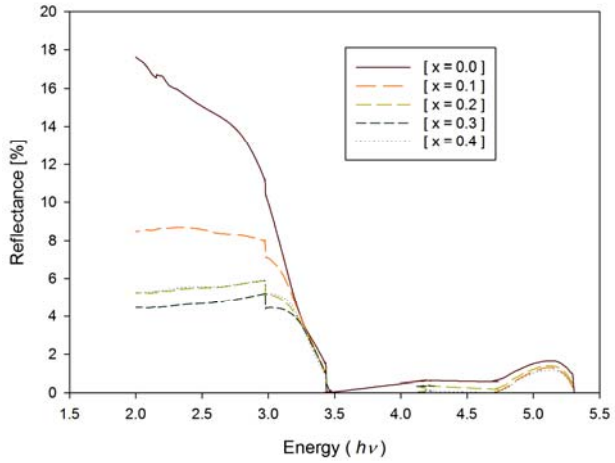

Fig. 4. Diffused spectra of Nickel doped ZnO nanoparticles with different concentration of Ni (i. e for x = 0.0 to 0.4).

The optical band gaps of pure and doped zinc oxide are estimated from the plots of reflectance verses energy. The band gap estimated for pure zinc oxide 3.42 eV that is slightly higher than the bulk zinc oxide (3.37 eV). The diffused reflectance spectra of Ni doped zinc oxide (Zn_{1-x} Ni_x O, where (x = 0.1 to 0.4)) shows that, as the concentrations of nickel increases (x = 0.1 to 0.4), the band gaps also increases. The band gap values were deduced from the intersection of the two linear regions Table 3.

Table 3. Variations of Optical band gap of Nickel doped ZnO nanoparticles with different concentration of Ni i.e (a) $Ni_{0.1}$ -doped ZnO- NPs, (b) $Ni_{0.2}$ - doped ZnO- NPs, (c) $Ni_{0.3}$ -doped ZnO –NPs, (d) $Ni_{0.4}$ -doped ZnO NPs at 500^0C .

Compound	Band gap (eV)
ZnO	3.42
$Ni_{0.1}Zn_{0.99}O$	3.47
$Ni_{0.2}Zn_{0.98}O$	3.49
$Ni_{0.3}Zn_{0.97}O$	3.50
$Ni_{0.4}Zn_{0.96}O$	3.51

Diffused spectra indicate that the Ni- doping causes little structural disorder in the Zinc oxide lattice. With the increased concentration of Nickel, more and more Ni^{+2} replace the position of Zn^{+2} and resulted in widening of the band gap (Table3). The widening of band gap in case of heavily doped semiconductors is due to the blocking of the low energy transitions by the donor electrons occupying the states at the bottom of the conduction band, which is known as Burstein- mass effect [20]

4. Conclusion

In this work, nanocrystals of pure and nickel doped ZnO with different concentration (0.1 to 0.4) at 500^0C were synthesized by using a hydrothermal method. The crystalline structure, morphology and optical properties were determined by XRD and UV- visible spectra. XRD analysis showed that the prepared samples are in hexagonal wurtzite phase. The particle size was analyzed by the size-strain plot method. The line broadening of ZnO –NPs and nickel doped ZnO with different concentration (0.1 to 0.4) at 500^0C was due to the lattice strain. Decreased strain values were observed for samples estimated with larger particle size. Widening of the band gap with increased Ni doping was also discussed with Burstein-mass effect. Thus based on enhanced optical and structural properties of Ni doped ZnO can be considered a suitable candidate for DSSC applications.

Acknowledgements

Authors are thankful to Dr. Atul Khanna, Department of Physics, Guru Nanak Dev University, Amritsar for his valuable suggestions and cooperation to avail X Ray diffraction and UV-Visible Spectrophotometer facilities.

References

[1] Zhong Lin Wang, J. Phys.: Condense. Matter **16,** R829 (2004).
[2] K. Nomura, H. Ohta, K. Ueda, T. Kamiya, M. Hirano, H. Hosono, Science, **300,** 1269 (2003)
[3] T. Nakada, Y. Hirabayashi, T. Tokado, D. Ohmori, T. Mise, Sol. Energy, **77,** 739 (2004)
[4] S. Y. Lee, E. S. Shim, H. S. Kang, S. S. Pang, J. S. Kang, Thin Solid Films, **437**, 31 (2005)
[5] R. Könenkamp, R. C. Word, C. Schlegel, Appl. Phys. Lett., **85,** 6004 (2004)
[6] N. Sharma, J. Kumar, S. Thakur, S. Sharma, V. Shrivastava, Drug Invention Today, **5**, 50 (2013)
[7] D. C Look, B. C. Ya, I. Alivov, S. J. Park, The future of ZnO light emitters. Physical status solid (a), (2004).
[8] S. J. Pearton, D. P. Norton, K. Ip, Y. W. Heo, T. Steiner, Progress in Materials Science, **50**(3) (2005)
[9] F. Quaranta, A. Valentini, F. R. Rizzi, G. Casamassima, J.Appl. Phys., **74**(1), 244 (1993).
[10] G. J. Fang, D. Li, and B. L. Yao, Thin Solid Films, **418**(2) 156 (2002).
[11] J. M. Verilhac, G. LeBlevennec, D. Djurado, F. Rieutord, M. Chouiki, J. P. Travers, A. Pron, Synthetic Metals, **156**(11-13), 815 (2006).
[12] D. A. Schwartz, N. S. Norberg, Q. P. Nguyen, J. M. Parker, D. R. Gamelin, J. Am. Chem. Soc. **125**, 13205 (2003).
[13] Dogan, Seydi, Ates, Aytunc, Xiong, Gang, Wilkinson, John, S. Tuzemen, M. Yildirim, R. T. Williams, Physical Status Solidi (A) Applied Research, **195**(1 SPEC), 165 (2003).
[14] Mirica, Eugenia, Reactive sputter deposition of piezoelectric zinc oxide thin films, in Chemical, Biochemical and Materials Engineering., Stevens Institute of Technology: New Jersey. (2002) 175.
[15] A. Hartmann, M. K Puchert, R. N. Lamb, Surface and Interface Analysis, **24**(9), 671 (1996).
[16] Basic Research Needs for Solar Energy Utilization, U.S. (2005).
[17] Y. Chiba, A. Islam, Y. Watanabe, R. Komiya, N. Koide, L. Han, Jpn. J. Appl. Phys. **45**, L638 (**2006)**.
[18] C. Y Chen, M. Wang, J. Y. Li, N. Pootrakulchote, L. Alibabaei, C. Ngocle, J. D. Decoppet, J. H. Tsai, C. Gra¨tzel, C. G. Wu, S. M. Zakeeruddin, M. Gra¨tzel, ACS Nano **3**, 3103 (2009).
[19] S Singh, N. Rama, M. S. R. Rao, Influence of d-d interband transitions on electrical resistivity in Ni doped polycrystalline ZnO. Appl. Phys. Letts. **88,** 222111 (2006)
[20] J. G. Lu, S. Fujita, T. Kawaharamura, H. Nishinaka, Y. Kamada, T. Ohshima, Z. Z. Ye, Y. J. Zeng, Y. Z. Zhang, L. P. Zhu, H. P. He, B. H. Zhao, Journal of Applied Physics, **101, 0**83705 **(**2007)

*Corresponding author: jiten.arni@gmail.com